Amorphous calcium carbonate based-microparticles for peptide pulmonary delivery

Frederic Tewes[1, 2], Oliviero L. Gobbo[1], Carsten Ehrhardt[1] and Anne Marie Healy[1*]*

1: School of Pharmacy and Pharmaceutical Sciences, Trinity College Dublin, Dublin 2, Ireland

2: INSERM U 1070, Pôle Biologie-Santé, Université de Poitiers, Faculté de Médecine & Pharmacie, 1 rue Georges Bonnet, 86022 Poitiers Cedex, France

E-mail: ftewes@univ-poitiers.fr; healyam@tcd.ie

Abstract

Amorphous calcium carbonate (ACC) is known to interact with proteins, for example in biogenic ACC, to form stable amorphous phases. The control of amorphous:crystalline and inorganic:organic ratios in inhalable calcium carbonate microparticles may enable particle properties to be adapted to suit the requirements of dry powders for pulmonary delivery by oral inhalation. For example, an amorphous phase can immobilise and stabilise polypeptides in their native structure and amorphous and crystalline phases have different mechanical properties. Therefore, inhalable composite microparticles made of inorganic (i.e. calcium carbonate and calcium formate) and organic (i.e. hyaluronan (HA)) amorphous and crystalline phases were investigated for peptide and protein pulmonary aerosol delivery. The crystalline:amorphous ratio and polymorphic form of the inorganic component was altered by changing the microparticle drying rate and by changing the ammonium carbonate and HA initial concentration. The bioactivity of the model peptide, salmon calcitonin (sCT), co-processed with alpha-1-antitrypsin (AAT), a model protein with peptidase inhibitor activity was maintained during processing and the microparticles had excellent aerodynamic properties, making them suitable for pulmonary aerosol delivery. The bioavailability of sCT after aerosol delivery as sCT and AAT-loaded composite microparticles to rats was 4-times higher than that of sCT solution.

Keywords

Amorphous calcium carbonate, composite microparticle, pulmonary inhalation, biomimetic process, peptide

1. Introduction

For peptides, polypeptides and proteins the lung is an attractive route into the bloodstream, owing to the high and thin surface area of the alveolar epithelium and due to lower metabolic activity compared to the gastrointestinal tract.[1] Peptide deposition within the lung can be controlled by the development of peptide-loaded microparticles with suitable aerodynamic properties that allow them reach the distal lungs, where the absorption capacity is higher. When developing a polypeptide formulation it is essential to prevent its degradation and unfolding. This protection can be provided by the presence of excipient(s) in an amorphous phase that immobilise and isolate peptide molecules in their native structure.[2] Ideally, in this vitrification-based stabilisation strategy, both polypeptide and excipient(s) are amorphous and miscible, forming a single amorphous phase, which should have a high glass transition temperature (T_g) in order to ensure stability at room temperature. According to Gordon and Taylor[3] the T_g of the composite glass will be intermediate to the T_g of the polypeptide and the excipient. Thus, the T_g of the excipient should be high in order to increase the T_g of the composite glass. In addition to vitrification, peptide-excipient interactions are important for polypeptide stabilisation.[4] These interactions should replace the hydrogen-bonds formed by water at the surface of polypeptide molecules, preserving their native structure. Consequently, the presence of excipients forming an amorphous phase with the polypeptide in the formulations can be very important to stabilise these molecules.[2]

Amorphous calcium carbonate (ACC) is an amorphous mineral phase which is known to interact with proteins and peptides, for example in biogenic ACC, to form stable amorphous phases.[5-6] No information about the T_g of ACC is found in the literature. An estimation of the T_g of dry materials can be made from the melting temperature of the crystalline phase, since studies have shown that the T_g is around 0.7-times the melting temperature. Vaterite, the more metastable crystalline calcium carbonate ($CaCO_3$) polymorph, converts to calcite upon heating at transition temperatures of 320–460°C, depending on the method of preparation.[7] If we assume, as a minimum, that the T_g of ACC is 0.7-times the phase transition temperature of vaterite to calcite, the T_g of ACC would be around 224°C, which is higher than the T_g of most excipients that are currently used to stabilise amorphous pharmaceutical solids. Therefore, having potentially a high T_g and being able to interact with proteins, we hypothesise

that ACC could be used to stabilise peptides in the formulation of inhalable particles. Qi et al.[8] similarly proposed ACC nanospheres for protein drug delivery.

Additionally, it has been shown that ACC can coexist with one of the $CaCO_3$ crystalline forms to produce material with advantageous specific properties.[9-12] Biominerals such as seashells,[9] eggshells[13] and bones[10, 14] are examples of hybrid materials composed of biopolymer and amorphous and crystalline minerals having high mechanical strength and light weight. Amorphous materials have the advantage of being isotropic and elastic, with no preferred growth directions so they can be more easily shaped.[5, 12, 15] On the other hand, crystalline $CaCO_3$ forms are less soluble but harder and more stable than their amorphous counterpart.[11] The combination of the two phases, amorphous and crystalline, may offer some advantageous properties to an inhalable powder. For example, materials with different proportions of amorphous and various polymorph crystalline phases could lead to different aerodynamic properties as well as different solubilities and dissolution rates.

Complex $CaCO_3$-based structures are created by invertebrates by using the highly soluble ACC and a biopolymer controlling the $CaCO_3$ polymorphic conversion.[9, 16-19] One way for the biopolymer to influence the shape of the mineral is by chemical interaction.[20] Hyaluronate (HA) polysaccharide may be used to facilitate particle formation. In fact, negatively charged carboxylic groups from HA could be used to interact with Ca^{2+} and control the nucleation of $CaCO_3$.[21] Furthermore, HA is a ubiquitous anionic polysaccharide that is part of the extracellular lung matrix and has already been investigated as an inhalable therapeutic agent for lung diseases.[22] For example, inhaled HA prevents the side effects of hypertonic saline inhalable solution, which is used to treat bronchiolitis and patients with cystic fibrosis.[22]

We hypothesise that inhalable microparticles could be made of ACC, crystalline $CaCO_3$ and biopolymer (HA), enabling their properties to be adapted in terms of aerodynamic characteristics, drug release profile, mechanical strength and protein stability. In particles of this type, the properties may be tuned by controlling the organic:inorganic material ratio and by controlling the solid state nature of the inorganic components. Therefore, we investigated the possibility of pulmonary delivery of salmon calcitonin (sCT) and alpha-1-antitrypsin (AAT), chosen as a model polypeptide and model protein, respectively, in the form of inhalable composite microparticles made of HA and $CaCO_3$.[23]

2. Results

The spray drying process developed produced spherical hollow particles (shells) with wall thickness of around 80 nm (**Figure 1**). The properties of these particles were tuned by altering three parameters: the spray drying inlet temperature, the concentration of HA and the concentration of ammonium carbonate ($(NH_4)_2CO_3$) in the spray dried feed solutions (**Table 1**).

Table 1: Composition and physical properties of the composite microparticles. (HA: hyaluronic acid sodium salt; D_{50} and span values describe the volume-weighted particle size distribution measured by laser diffraction)

	Formulation parameters				Results				
Code	$Ca(OH)_2$ ($g\ L^{-1}$)	HA ($g\ L^{-1}$)	$(NH_4)_2CO_3$ ($g\ L^{-1}$)	inlet/outlet temp (°C)	D_{50} (µm)	span $(D_{90}-D_{10})/D_{50}$	specific surface area ($m^2\ g^{-1}$)	True density ($g\ cm^{-3}$)	Ca loading % (Assay)
temp1	0.8	0.2	1.2	100/39	4.65 ± 0.5	2.11 ± 0.04	17.8 ± 1.2	1.25 ± 0.02	36.8 ± 2.3
temp2	0.8	0.2	1.2	110/44	4.55 ± 0.4	2.12 ± 0.08	16.5 ± 0.8	1.06 ± 0.07	38.7 ± 2.6
temp3	0.8	0.2	1.2	120/50	4.74 ± 0.3	2.07 ± 0.04	19.6 ± 0.8	1.37 ±0.01	34.3 ± 2.9
temp4	0.8	0.2	1.2	140/68	4.67 ± 0.4	2.10 ± 0.05	19.3 ± 0.6	2.06 ± 0.01	37.3 ± 3.2
Carb1	0.8	0.2	1.2	120/50	4.74 ± 0.3	2.07 ± 0.04	19.6 ± 0.8	1.37 ±0.01	34.3 ± 2.9
Carb2	0.8	0.2	2.4	120/50	5.48 ± 0.7	2.11 ± 0.10	30.1 ± 1.0	1.74 ± 0.03	57.3 ± 4.6
Carb3	0.8	0.2	4.8	120/50	7.07 ± 0.5	2.00 ± 0.06	28.0 ± 0.9	1.49 ± 0.06	65.2 ± 3.1
Carb4	0.8	0.2	6	120/50	5.34 ± 0.3	2.26 ± 0.11	23.6 ± 0.8	2.26 ± 0.06	53.5 ± 4.0
HA1	0.8	0.1	1.2	120/50	5.36 ± 0.4	1.84 ± 0.05	18.7 ± 0.6	2.35 ± 0.05	48.9 ± 2.9
HA2	0.8	0.2	1.2	120/50	4.74 ± 0.3	2.07 ± 0.04	19.6 ± 0.8	1.37 ±0.01	34.3 ± 2.9
HA3	0.8	0.4	1.2	120/50	7.45 ± 0.5	2.07 ± 0.07	17.7 ± 0.7	1.10 ± 0.05	34.6 ± 3.5
HA4	0.8	0.6	1.2	120/50	10.20 ± 0.6	2.19 ± 0.08	15.7 ± 0.8	1.21 ± 0.10	32.0 ± 4.1

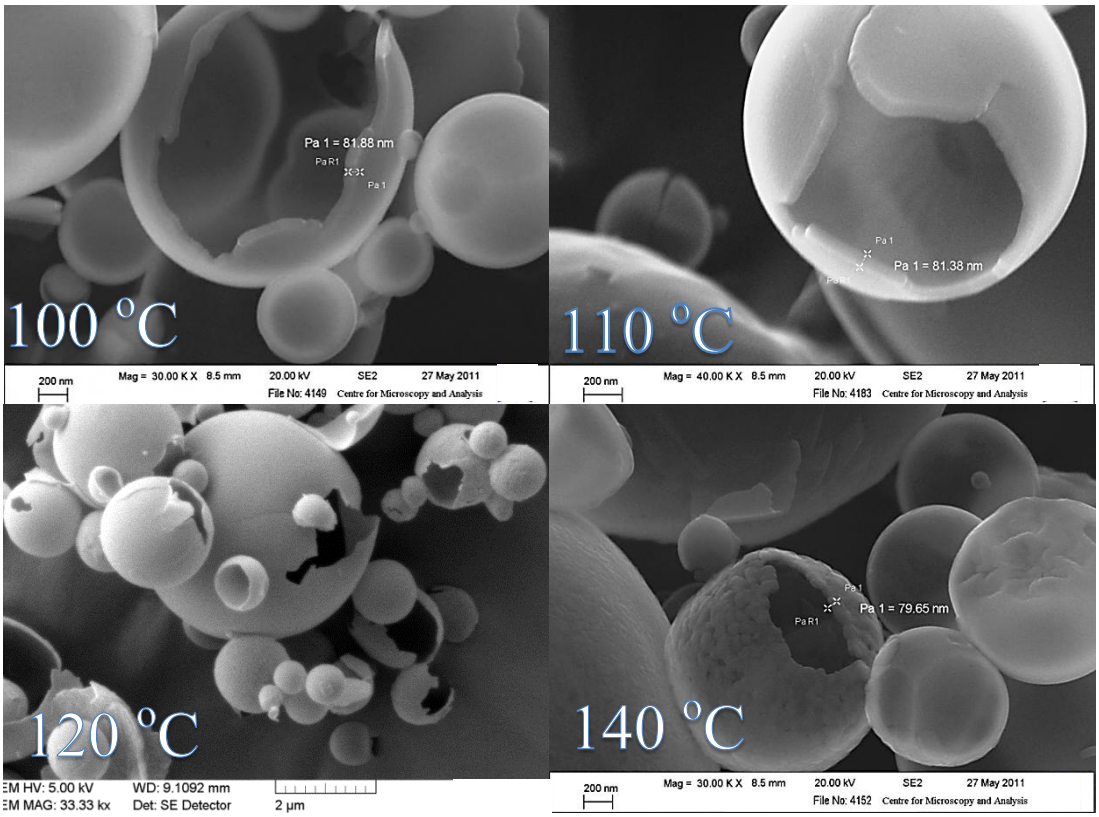

Figure 1: SEM micrographs of Ca/HA composite microparticles formulated at different spray drying inlet temperatures (T_{inlet}).

2.1. Processing temperature effect

Changing the spray drying inlet temperature (T_{inlet}) in the 100 °C – 140 °C range did not alter the particle morphology (**Figure 1**) or particle size distribution (**Table 1**). The formulations had a volume median geometric diameter (D_{50}) of 4.6 ± 0.4 µm and high specific surface area values (16.5 to 19.6 $m^2\ g^{-1}$). The calcium concentration in the particles was not modified, but the true density of the particles changed with the T_{inlet} (Table 1), indicating a change in their composition or in their solid state. The solid state of the powders was determined by XRD measurements performed immediately after production (**Figure 2**). Powders formulated at a T_{inlet} of 100 °C showed just a diffuse halo in the XRD pattern, characteristic of XRD amorphous material (**Figure 2A**). An increase in T_{inlet} from 110 °C up to 140 °C led to the appearance of low intensity diffraction peaks ascribed to crystalline calcium formate ($Ca(HCOO)_2$).[24] The presence of $Ca(HCOO)_2$ resulted from the reaction between the calcium hydroxide $Ca(OH)_2$ and formic acid (HCOOH) that was initially present in the solutions.

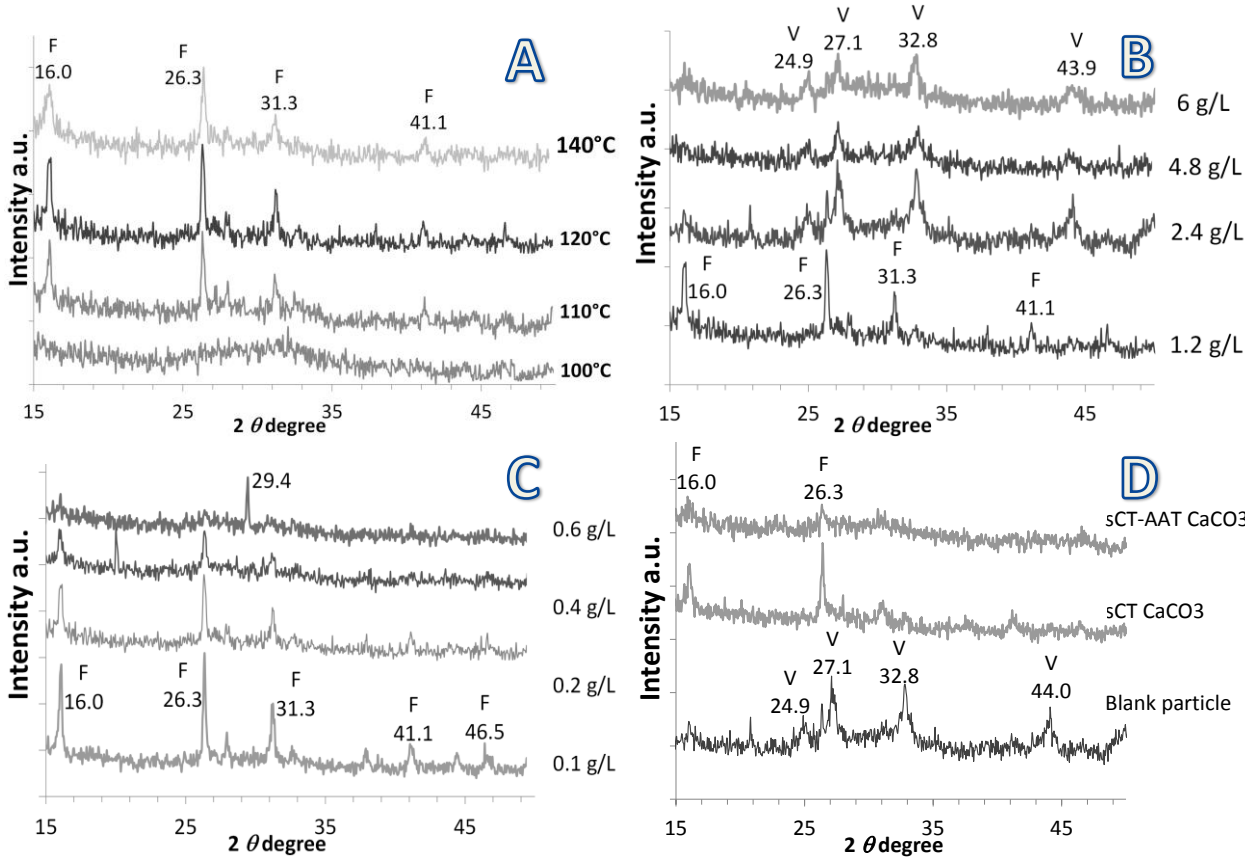

Figure 2: XRD patterns of Ca/HA composite particle: A) Formulated at different temperatures, B) Formulated at different concentrations of $(NH_4)_2CO_3$, C) Formulated at different concentrations of HA, D) Loaded with sCT and AAT. (F) label is for calcium formate, (V) label is for vaterite $CaCO_3$ polymorph and (C) is for calcite $CaCO_3$ polymorph.

Fourier transform-infrared (FTIR) spectroscopy was used to investigate the chemical nature of the particles (**Figure 3A**). All spectra presented absorption bands typical of carbonate and carboxylate.[25-26] The absence of the carbonate absorption bands at 700, 713 and at 745 cm^{-1} [26] in the spectra indicates the absence of detectable anhydrous crystalline $CaCO_3$ polymorphs. However, ACC spectra are characterised by a broad band of the carbonate bending at 866 cm^{-1} and a split in the asymmetric stretch of the carbonate ion at 1417 and 1488 cm^{-1}.[11, 20, 27-28] Carbonate absorption bands recorded for the microparticles formulated at T_{inlet} of 100 °C have maximal values typical of ACC, confirming the XRD data.

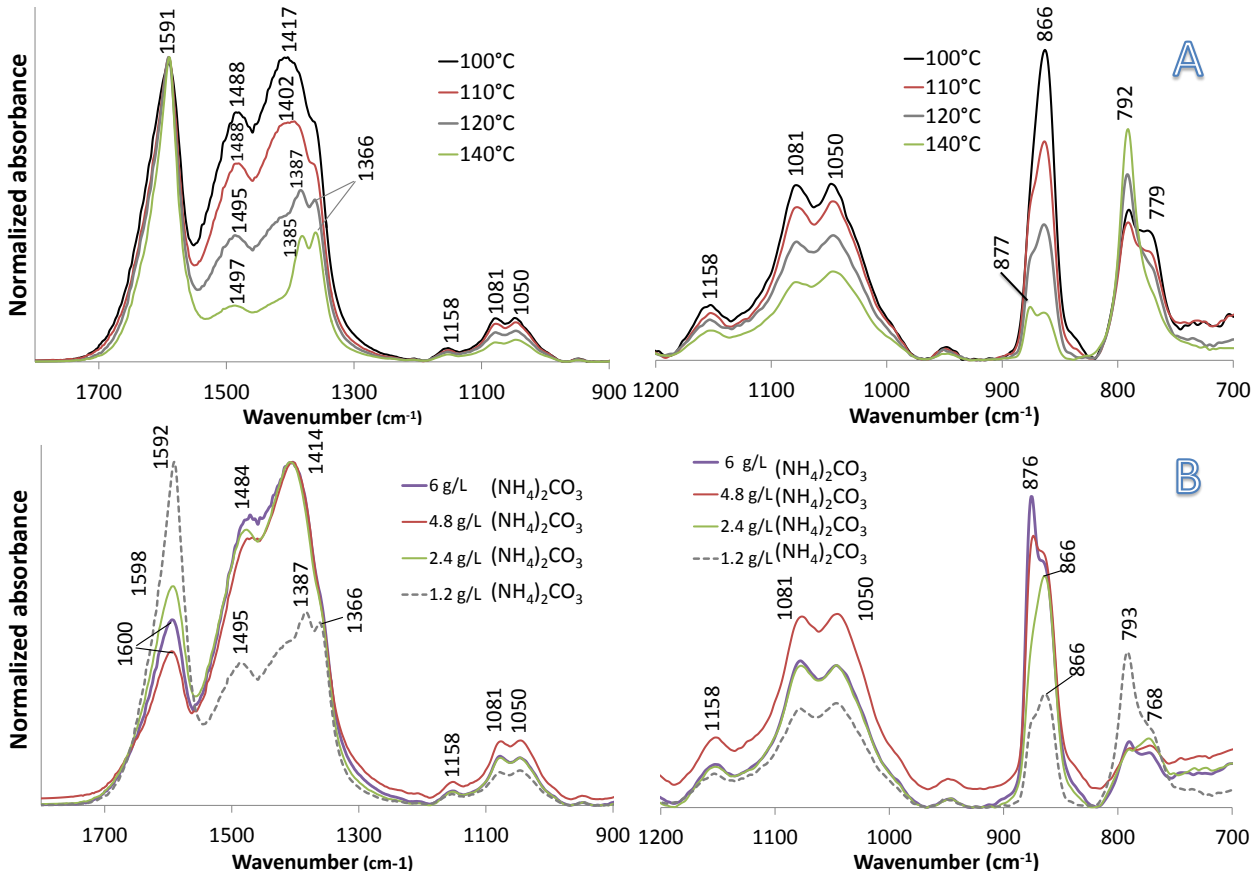

Figure 3: FTIR spectra of Ca/HA composite microparticle A) Formulated at different temperatures, B) Formulated at different concentrations of $(NH_4)_2CO_3$.

An increase in T_{inlet} resulted in a reduction in the intensity of bands typical of ACC. When processed at T_{inlet} = 140 °C, the 866 cm^{-1} band was split, with a sharper peak at 877 cm^{-1}, indicative of the possible presence of some crystalline calcite or vaterite in addition to the ACC.[27] The bands at 1591 cm^{-1} and 792 cm^{-1} can be attributed to the asymmetric stretch and the bending of the carboxyl group of calcium formate.[25, 29] The relative intensity of these bands increased with an increase in T_{inlet}, suggesting an increase in calcium formate concentration in the particles.

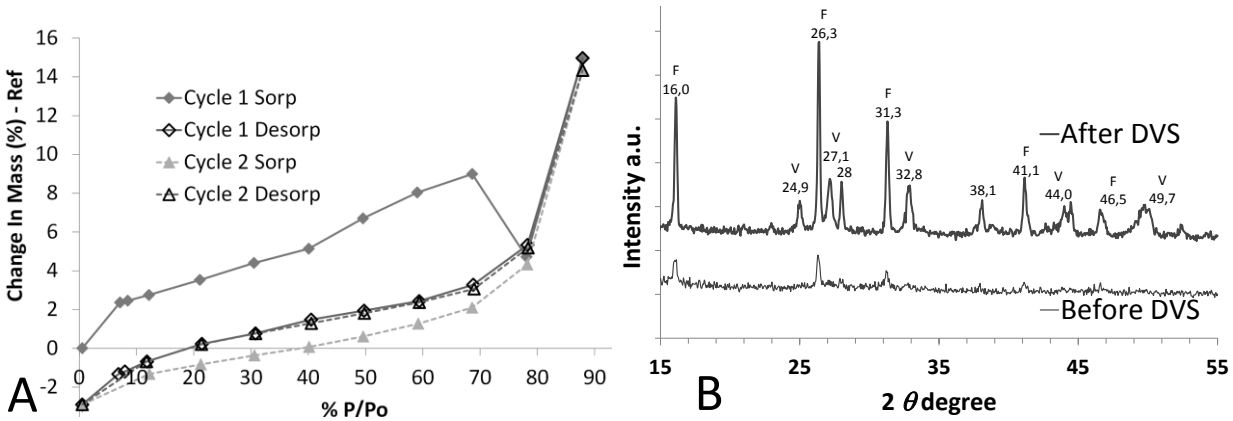

Figure 4: A) Water sorption isotherms (at 25 °C) of Ca/HA composite microparticles formulated at 120 °C (temp3). B) XRD patterns recorded before and after DVS experiment. (F) label is for calcium formate and (V) label is for vaterite $CaCO_3$ polymorph.

For amorphous solids, the interactions with water are fundamental aspects to be studied because they can affect both dissolution properties and physical stability.[30] The water sorption-desorption isotherm of composite microparticles formulated at 120 °C (temp3) showed a water mass increase of 10 % (w/w) with an increase in RH up to 70 %, followed by a mass decrease for the 70 to 80 % RH step (**Figure 4A**). A decrease in mass with increasing RH for amorphous substances corresponds to crystallisation of the material.[31-33] XRD diffractograms of the formulation temp3 measured after the DVS experiment (**Figure 4B**) showed new diffraction peaks characteristic of the vaterite $CaCO_3$ polymorph[34-35] and an increase in the intensity of the peak corresponding to calcium formate. Therefore, the crystallisation which occurred during water sorption corresponds to further crystallisation of calcium formate and to the crystallisation of the ACC to vaterite. The second water sorption-desorption cycle did not show any sign of further crystallisation or polymorphic change.

2.2 Ammonium carbonate concentration effect

Changing the $(NH_4)_2CO_3$ feed solution concentration did not alter particle morphology, as observed by SEM (supporting information Figure S4), but changed their physicochemical properties (Table 1). An increase in $(NH_4)_2CO_3$ from 1.2 g L^{-1} to 4.8 g L^{-1} resulted in a 2-fold increase in the specific surface area, and increased the calcium concentration in the particles from 38.7 ± 2.6 % to 65.2 ± 3.1 %, respectively. True density changed variably with the $(NH_4)_2CO_3$ concentration but increased markedly to 2.26 ± 0.06 g cm^{-3} for 6 g L^{-1} of $(NH_4)_2CO_3$. This density is higher than that of calcium formate (2.009 g cm^{-3}), and closer to the density of pure $CaCO_3$ (vaterite 2.645 g cm^{-3}, calcite 2.711 g cm^{-3}).[36] Analysis of the effect of $(NH_4)_2CO_3$ concentration on the particles properties by XRD (Figure 2B) and ATR-FTIR (Figure 3B) showed solid state changes. For a concentration of 1.2 g L^{-1} in $(NH_4)_2CO_3$ only the XRD Bragg peaks specific to calcium formate were observed. An increase in $(NH_4)_2CO_3$ concentration in solution to higher than 1.2 g L^{-1} induced the formation of vaterite (Figure 3B). From 2.4 g L^{-1} to 6 g L^{-1} only Bragg peaks characteristic of vaterite were observed.

FTIR spectra of particles formulated at low $(NH_4)_2CO_3$ concentration (Figure 3B) were characterised by a broad band of the carbonate bending at 866 cm^{-1}, which is typical of ACC.[27] An increase in $(NH_4)_2CO_3$ concentration in the spray dried feed solution to higher than 1.2 g L^{-1} induced a shift of this band to 876 cm^{-1}, which is characteristic of calcite or vaterite.[35] The bands split at 1414 and 1484 cm^{-1}, which is characteristic of the asymmetric stretch of the carbonate ion[11, 27, 37], increased with the

$(NH_4)_2CO_3$ concentration increase, while the asymmetric stretch at 1592 cm^{-1} and the bending at 793 cm^{-1} of the carboxyl ion of calcium formate[25] decreased in intensity, confirming the decrease in calcium formate concentration in the particles, as was suggested by XRD.

2.3 Hyaluronan concentration effect

The major change induced by the increase in HA concentration was an increase in particle size, for HA concentrations higher than 0.2 g L^{-1}, and a decrease in particle density and calcium concentration (Table 1). The increase in particle size could be attributed to the increase in the feed solution viscosity, producing larger droplets in the spray dryer. Particle morphology, as observed by SEM, was similar for the various HA concentrations (Supporting Information Figure S5).

The intensities of the diffraction peaks on the XRD patterns were low, suggesting that the formulations were mostly amorphous (Figure 2C). However, an increase in HA concentration from 0.1 g L^{-1} to 0.6 g L^{-1} changed the solid state nature of the material. For HA concentrations ranging from 0.1 g L^{-1} to 0.4 g L^{-1} only diffraction peaks characteristic of calcium formate were observed. The intensity of these peaks decreased with an increase in HA concentration, suggesting a decrease in concentration or in crystallinity of calcium formate in the particles. At a HA concentration of 0.6 g L^{-1}, a diffraction peak at 29.4^o (2θ), specific to the $CaCO_3$ polymorph, calcite, was observed.[34-35] The major change observed on FTIR spectra (Supporting Information Figure S2) induced by an increase in HA concentration was a decrease in intensity of the calcium formate carboxyl band at 793 cm^{-1}, [25] suggesting that the increase in HA concentration inhibited the formation of calcium formate in the particles. [38]

2.4 Salmon calcitonin-loaded microparticles

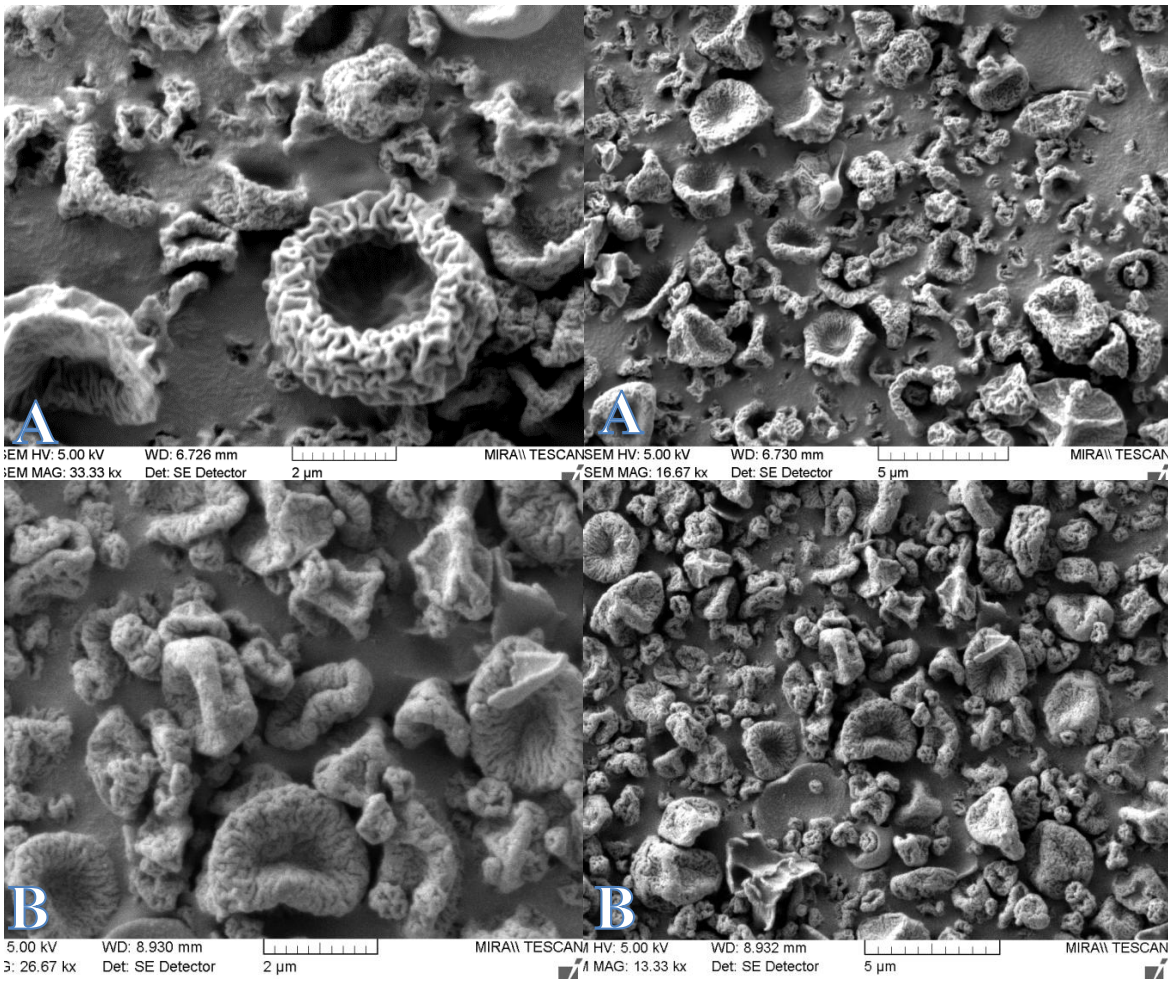

Figure 5: SEM micrographs of Ca/HA composite particles loaded with sCT (A) and sCT and AAT (B).

In this study, sCT was chosen as a model peptide which is sensitive to pulmonary peptidase, limiting its pulmonary bioavailability (F%). To achieve higher F%, sCT was co-administrated with AAT to provide protection from lung peptidases. AAT is a 52-kDa protein produced by the liver, the main physiological function of which is the inactivation of proteolytic enzymes in pulmonary tissue. Inhaled AAT has been shown to be suitable for the treatment of AAT deficiency and is currently in clinical trials.[23] However, AAT has not yet been used to protect inhaled peptides against degradation and could be an interesting new approach.

sCT and sCT-AAT-loaded microparticles were formulated by adding sCT or sCT and AAT to the Carb2 formulation, which was principally composed of amorphous materials (Table 1). This formulation was chosen, not only because of its amorphous composition, but also based on the high specific surface area and low D_{50}, suggesting good aerodynamic properties and fast drug release. The

addition of sCT alone (0.4 g L^{-1}) or AAT (0.2 g L^{-1}) and sCT (0.2 g L^{-1}) in the composite microparticles totally changed their morphology, as observed by SEM (**Figure 5**). Blank particles were hollow shells, but became crimpled basket-shaped particles in the presence of sCT or sCT-AAT. For the sCT particles, the sCT loading was 24.6 ± 2.4% (w/w). The maximal sCT theoretical loading (calculated by considering the complete elimination of the volatile compounds during the spray-drying process) is 23.8 % (w/w) (see experimental procedures). Therefore, the sCT loading efficiency was close to 100%. For the sCT-AAT-loaded microparticles, the sCT loading was 9.0 ± 0.8% (w/w/) and the maximal theoretical sCT loading is 11.9 % (w/w), suggesting a loading efficiency between 69 % and 82%.

Again, XRD patterns for all formulations had very low intensity diffraction peaks, indicating a low degree of crystallinity in the particles. The only residual diffraction peaks recorded for the blank particles indicated the presence of vaterite (Figure 2D). The XRD pattern of the sCT-loaded particles showed only low intensity peaks specific to calcium formate. The formulations containing both sCT and AAT were completely XRD amorphous. Analysis by FTIR showed that the incorporation of sCT in the formulation increased the intensity of the bands assigned to calcium formate and decreased the intensity of the band characteristic of ACC (Supporting Information Figure S2). The combined addition of sCT and AAT resulted in an increase in intensity of the FTIR band characteristic of ACC, which was consistent with the XRD results.

As was the case for the blank particles, the water sorption-desorption isotherm of sCT-AAT-loaded microparticles (supplementary information Figure S6) showed mass increase with an increase in RH up to 70%, followed by a mass decrease for the 70 to 80% RH step. The XRD patterns of sCT and sCT-AAT-loaded formulations recorded after a full water sorption-desorption isotherm showed diffraction peaks specific to vaterite and calcium formate of higher intensity than before the DVS cycle. Thus, as for the blank particles, two crystallisation processes occurred at 80% RH, the crystallisation of vaterite from ACC and an increase in crystalline calcium formate.

Aerodynamic analysis of the sCT-AAT-loaded microparticles showed optimal properties for lung inhalation when using a dry powder inhaler (Supporting information Figure S7). sCT-AAT-loaded particles emitted from the dry powder inhaler had a mass median aerodynamic diameter of 2.89 ± 0.23

µm with a geometric standard deviation of 1.82 ± 0.16. The fine particle fraction (i.e. the fraction of particles that are capable of penetrating and depositing within the lungs) expressed as per the emitted recovered dose, was 64.1 ± 7.1 %.

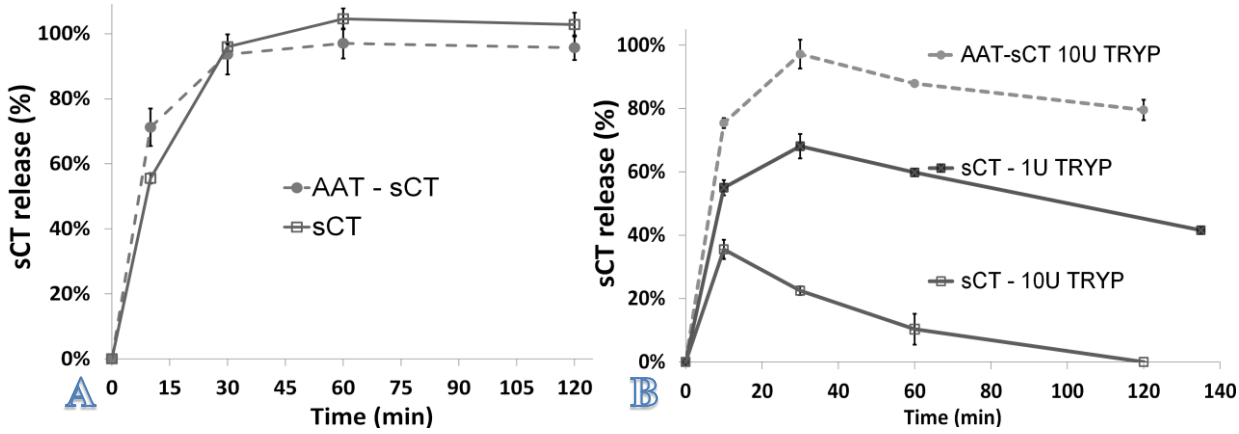

Figure 6: sCT release from sCT and sCT-AAT-loaded microparticles in the absence (A) or in the presence (B) of trypsin in the PBS pH 7.4. Temperature was 37°C.

sCT release from sCT or sCT-AAT-loaded microparticles was complete after 30 min in PBS pH 7.4 (**Figure 6A**). Both formulations showed the same fast release profile. In the presence of trypsin in the release buffer, sCT was rapidly degraded, leading to a reduction in intact sCT released from sCT-loaded particles, with the rate of degradation increasing with the trypsin concentration (**Figure 6B**). In the presence of 10 U (BAEE units) of trypsin in the buffer, all the sCT released from the sCT-loaded particles was degraded after 2 h. For sCT release from sCT-AAT-loaded microparticles, higher proteolytic stability was observed and 85 % of the sCT initially loaded in the particles was detected in the buffer containing 10U of trypsin after 2 h. These results suggest that the AAT protein that was present in the particles was still active and able to protect sCT from degradation.

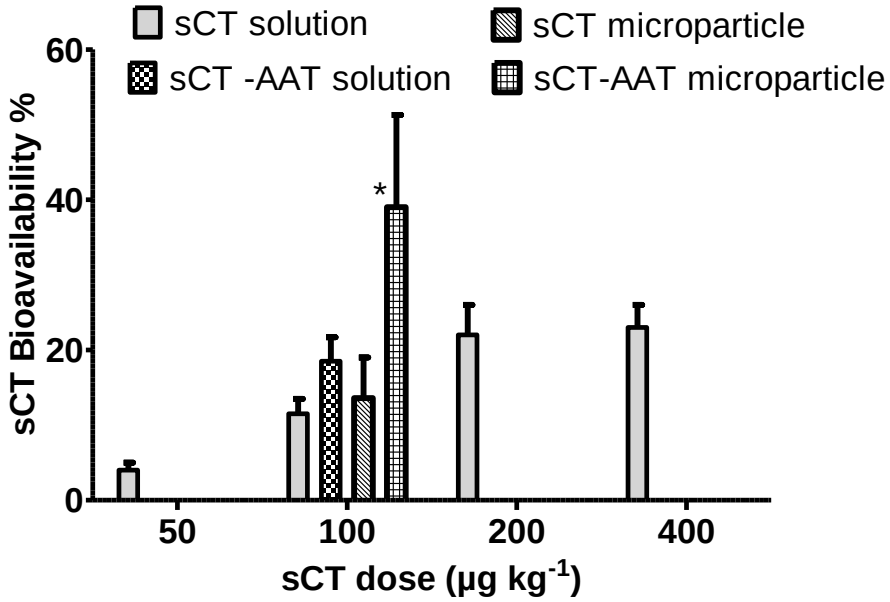

Figure 7: sCT bioavailability (F) after pulmonary administration of various sCT dose by nebulising 100 µL of sCT solutions at different concentration or by inhaling sCT or sCT-AAT microparticle to rats. (mean ± SEM (n = 2-7)) For the sCT dose of 100 µg kg^{-1}, * indicates a significant difference between the mean bioavailability of the formulations compare to those obtained with pure sCT solution nebulisation (P < 0.05). One-way ANOVA test performed on the set of data obtained by nebulising sCT solutions at different concentrations showed a significant increase in sCT bioavailability with an increase in the sCT dose in the range 50 – 200 µg kg^{-1}, but no difference was observed between the 200 and 400 µg kg^{-1} doses.

sCT displayed nonlinear pulmonary pharmacokinetics (PK) in rat and increasing the sCT dose by nebulising sCT solutions of increasing concentration changed the sCT bioavailability (**Figure 7**). At a low dose (50 µg kg^{-1}) pulmonary sCT bioavailability from a nebulised solution was low (4 %), and increased with increasing dose to plateau at around 23 % for doses of 200 and 400 µg kg^{-1}. Also, increasing the sCT dose increased T_{max} from 5 min for a dose of 50 µg kg^{-1} up to 15 min for a dose of 200 µg kg^{-1}. The non-linear sCT PK following pulmonary administration was not due to a change in sCT plasma elimination, as sCT PK following i.v. administration was linear in this dose range (50 - 400 µg kg^{-1}). Likewise, sCT demonstrated linear PK following i.v. administration of 1, 5 and 10 µg doses in rats.[39] However, PK obtained after sCT i.v. administration in dogs were non-linear over a higher dose range (1-1000 µg).[39]

Average sCT plasma concentration-versus-time profiles were different after pulmonary administration of a solution of sCT alone (100 µg kg^{-1}) compared to when sCT was combined with AAT in solution (**Figure 8A**). For sCT alone, sCT lung absorption was fast, with a T_{max} of 4.2 ± 1.1 min, followed by a fast elimination leading to a bioavailability (F) of 11.9 ± 3.9 %.

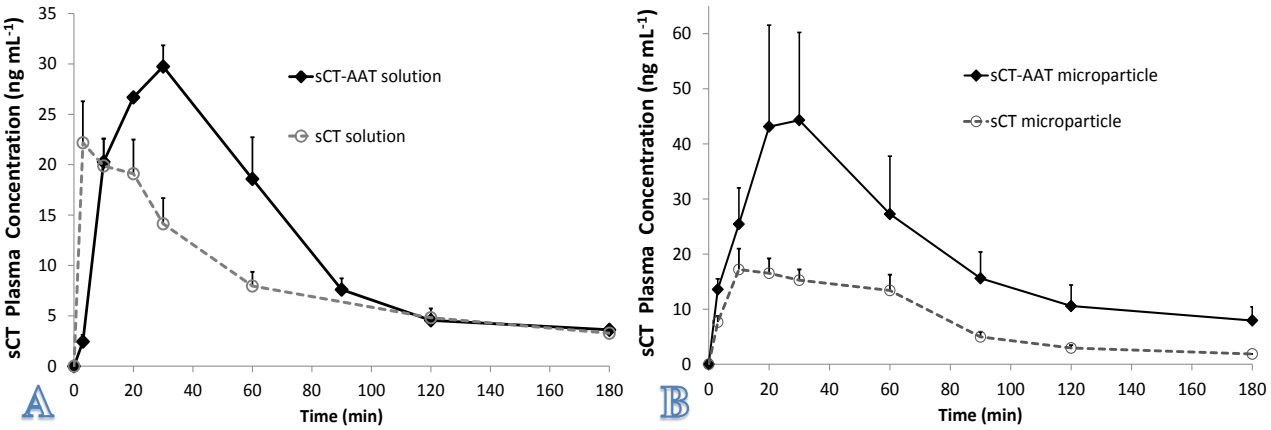

Figure 8: sCT plasma concentration-versus-time profiles after: A) sCT solution nebulisation B) sCT-loaded composite microparticles inhalation (mean ± SD). Dose 100 µg Kg^{-1}.

In the presence of AAT, sCT bioavailability was not significantly changed. However, T_{max} was shifted to 30 ± 0.1 min and the systemic absorption was slowed down in comparison to the pure sCT solution, as described by the lower absorption constant, K_a = 0.128 ± 0.002 min^{-1} (**Table 2**).

Administration of sCT as composite microparticles (without AAT) increased only the absorption T_{max} but other all pharmacokinetic parameters were identical to those obtained with pure sCT solutions. This increase in T_{max} should be related to the time taken for sCT to be released from the particles. With the addition of AAT to the particles, most of the pharmacokinetic parameters were significantly changed. C_{max}, T_{max} and AUC of sCT plasma concentration-versus-time profiles were increased, leading to a 4-times increased sCT bioavailability compared to sCT solution (Figure 7 and 8B).

Table 2: Pharmacokinetic parameters of the sCT plasma concentration versus time profiles. (mean ± SD (n = 2-7)); * P < 0.05, indicates a significant difference between the mean values of the PK parameters compared to those obtained for sCT solution pulmonary administration. AUC ∞ is the area under the sCT plasma concentration versus time curve. T_{max} is the time of peak sCT plasma concentration. C_{max} is the maximal sCT plasma concentration obtained at T_{max}. ka is the first order absorption rate constant. F (the bioavailability) is the fraction of the dose which is absorbed.

	sCT solution	sCT AAT solution	sCT composite microparticles	sCT-AAT composite microparticles
AUC ∞ (min ng mL^{-1})	1493 ± 526	2319 ± 397	1705 ± 549	4907 ± 3085*
Tmax (min)	4.2 ± 1.1	30.0 ± 0.1	16.6 ± 4.7	23.3 ± 4.7*
Cmax (ng mL-1)	24.1 ± 4.5	31.4 ± 1.3	18.0 ± 6.2	46.8 ± 30.3*
K_a (min^{-1})	0.476 ± 0.152	0.128 ± 0.002*	0.188 ± 0.027*	0.155 ± 0.025*
F(%)	11.9 ± 3.9	18.5 ± 3.2	13.6 ± 5.4	39.2 ± 24.6*

3. Discussion

In many living entities, solid $CaCO_3$ is shaped into different structures to adapt and fulfil different functions.[11] Eggshell and bones are examples of $CaCO_3$-made structures which are light and have good mechanical resistance. In this study, we attempted to use these properties to formulate microparticles for pulmonary peptide delivery. We showed that shell-like inorganic-organic inhalable microparticles could be made of $CaCO_3$, calcium formate and biopolymer (HA) with properties matching the pharmaceutical requirements of an aerosolisable powder. In this process, the microparticle properties were tuned by different means, i.e. by altering the drying temperature, the $(NH_4)_2CO_3$ and HA concentration in the spray dried feed solutions. For an inhalable peptide or protein-loaded particle formulation, the main objective is to obtain a high content of amorphous phase in order to stabilise the peptide/protein in its native structure. Also, these particles should reach the deep lung, the region of most efficient protein absorption. Therefore, a narrow particle size distribution in the range 3- 6 µm and a specific surface area higher than 20 $m^2 g^{-1}$ were also targeted parameters.

Increasing the spray drying temperature, which increases the rate and extent of drying[40] had several effects on the particles' properties. Firstly, it favoured the formation of calcium formate ($Ca(HCOO)_2$)

over the formation of $CaCO_3$. Secondly, it impacted on the solid state of these two chemicals ($Ca(HCOO)_2$ and $CaCO_3$). Calcium formate was present in the particles in the crystalline and/or amorphous state. To our knowledge, this is the first report of amorphous calcium formate. Spray drying is a process which often produces amorphous pharmaceuticals. The ratio between amorphous and crystalline calcium formate depended on the spray drying temperature. At low drying temperature (100 °C) the particles were fully amorphous. An increase in temperature up to 140 °C led to the increased formation of crystalline calcium formate phase. $CaCO_3$ was XRD amorphous at all processing temperatures used. However, for the particles produced at 140 °C, FTIR experiments suggested the presence, in low proportions, of a calcium carbonate phase which was more organised than ACC. $CaCO_3$ can solidify as three anhydrous crystalline polymorphs (calcite, aragonite, vaterite), two hydrates (hexahydrate and monohydrate) and ACC, which is the most thermodynamically unstable.[16] Stable ACC can be obtained by the addition of different excipients, such as polymers, to the solid phase[17, 41-42] and by controlling the amount of water present in the solid phase (hydrated ACC). This last phenomenon was mainly observed with ACC produced in living organisms.[5] Water present in $CaCO_3$ lowers the energy barrier towards the solidification of hydrated ACC compared with the anhydrous crystalline forms.[28, 43] Also, maintaining this hydration could be important for stability of the ACC, as crystallisation induced by heat is thought to involve dehydration of hydrated ACC.[19, 28, 36, 44-46] Likewise, ACC crystallisation can be retarded by providing a barrier to water loss.[28] In a pharmaceutical context, water is usually considered to be a plasticiser, decreasing the T_g of an amorphous solid and increasing the local molecular mobility and physical instability. It is generally recognised that exposure to water has to be avoided in order to obtain stable amorphous pharmaceutical solids; thus the behaviour of ACC appears to be an exception.

At ambient temperature, as for the polymorphic transformation of crystalline $CaCO_3$, ACC crystallisation is triggered through local superficial ACC dissolution in surface water and local crystallisation to form nucleation clusters.[28] Surface water is thus important for this dissolution-crystallisation process to occur. For example, ACC washed with ethanol to remove surface water or ACC prepared by freeze drying that has no surface water shows extended stability.[47-48] The conversion of the ACC into the vaterite crystalline phase observed when the relative humidity was increased

above 70% should be related to the local dissolution of ACC in adsorbed and absorbed water. Recent work suggests that vaterite is often the first phase to form during crystallisation of pure ACC.[44-45] However, this is not a generalised result and depends on how the ACC is prepared.[49] Aqueous solubility of hydrates is generally lower than the anhydrous form.[50] Therefore, the dissolution-crystallisation process needed to crystallise $CaCO_3$ could be favoured for anhydrous compared to hydrated ACC. Thus, avoiding the complete dehydration of $CaCO_3$ during the solidification step, by adjusting the T_{inlet}, seems to be important in the formulation of stable ACC by spray drying. Controlling the spray drying temperature, water evaporation rate and residual amount of water in the final particles could be a way of forming stable amorphous/crystalline composite particles. $CaCO_3$ may not be exclusively involved in this crystallisation process and this may happen for calcium formate also.

Changing HA and $(NH_4)_2CO_3$ concentrations had several consequences on the nature of the particles' inorganic component. Firstly, increasing HA and $(NH_4)_2CO_3$ concentrations facilitated the formation of $CaCO_3$ over calcium formate. Secondly, HA and $(NH_4)_2CO_3$ concentrations influenced the solid state nature of the $CaCO_3$. High HA concentrations induced the formation of calcite, the stable $CaCO_3$ polymorph. Negatively charged carboxylic groups of HA polymers are assumed to be responsible for nucleation of this particular $CaCO_3$ polymorph by interacting with calcium ions.[51] In fact, HA was previously shown to facilitate and control the formation and shape of calcite.[21] Also, it has been shown that $CaCO_3$ polymorphic transformations proceeded by the dissolution of the metastable phases and the growth of calcite, and that the rate-determining step was the growth of calcite.[46] An increase in HA concentration results in an increase in solution viscosity and slows down the mobility of the Ca^{2+} and CO_3^{2-} ions. This reduction of the ions' mobility should favor the thermodynamic over the kinetic control of the crystallisation process, leading to the formation of the stable calcite. In fact, an increasing proportion of calcite over vaterite was previously observed for $CaCO_3$ growth in solution for solutions with viscosities above 1.6 mPa s.[52]

Increasing $(NH_4)_2CO_3$ concentration facilitates the formation of the vaterite phase. Changing $(NH_4)_2CO_3$ feed solution concentration had a direct effect on carbonate ion concentration. A previous study showed that the carbonate ion concentration had a kinetic control on the growth of $CaCO_3$,

facilitating the formation of vaterite as the carbonate ion concentration increased for a given calcium ion concentration.[53] The control of the solid state nature and composition of the inorganic component of the particles enables their physicochemical properties to be adapted to best suit the requirements of pharmaceutical dry powders for inhalation. It is evident that changes in the solid state forms (ACC, vaterite, calcite, calcium formate), could also impact the particles stability, porosity, immobilisation capacity of peptides/proteins and loading efficiency. The most physically stable particles are expected to be those comprised of calcite, the stable form of $CaCO_3$. The least stable formulation is expected to be that comprised of ACC. However ACC can be stabilied when stored with no surface bound water,[47] and the long-term stability of this formulation might not be a problem. Maintenance of protein native structure is usually performed using the amorphous phase.[2] However, lysozyme-loaded vaterite microspheres showed good maintenance of the activity of encapsulated protein.[54] Porosity and specific surface area are important characteristics to maximise in the production of inhalable particles, and vaterite and AAC particles often present high specific surface areas.[54]

In order to reach the pulmonary alveoli, particles must have an aerodynamic-equivalent diameter (d_a) in the 1–5 μm range.[56] d_a is linked to the volume-equivalent geometric diameter (d_g) of the particles by the particle shape, evaluated by the particle shape factor (χ), and by the particle density (ρ_p).[57-58] χ is defined as the ratio of the drag force on a particle to the drag force on a volume-equivalent sphere at the same velocity.[58] In order to decrease the d_a of geometrically large particles to below 5 μm, several studies focused on enhancing the particle porosity and specific surface area, while maintaining small contact area between particles, to increase χ and decrease ρ_p.[32-33, 59-61] All blank particles produced in the current study were shell-like and had high specific surface areas compared to solid spherical particles of the same size.[61] The incorporation of sCT in the formulation completely changed the particle morphology to wrinkled particles. This new morphology is especially well-suited to pulmonary drug delivery as the presence of a rough surface results in an increase in χ but a reduction in the inter-particle contact area.[56] The mass median aerodynamic diameter (MMAD) of particles considered suitable for topical respiratory treatment is between 1 and 5 μm. However, the optimum size to reach the alveoli is between 2 and 3 μm.[55] Particles with a MMAD from 3 to 5 are deposited predominantly in the conducting airways. The MMAD of 2.89 ± 0.23 μm, which was determined for

the sCT-AAT-loaded particles, suggests that these particles should mainly reach the alveoli, where the absorption capacity of the lung is the highest.

The morphology of particles produced by spray drying can be explained by the material's Peclet number (*Pe*).[59] The Peclet number compares the diffusion rate of the solute and the evaporation rate of the receding droplet surface. For materials with a *Pe* larger than 1, i.e. moving slowly in the liquid, the sprayed droplet surface moves faster than the dissolved or suspended material, resulting in material accumulation and solidification at the surface. The resulting particles can be hollow spheres if the shell becomes rigid quickly, as occurred for the blank particles. If the surface is soft, it can buckle or fold on the internal and external void space to form a wrinkled or dimpled morphology, as was observed for the particles containing sCT. sCT appears to make the particle wall softer, leading to the formation of wrinkled particles. In fact sCT has a T_g around 147 °C[62], which should be lower than the T_g of ACC and make the particle wall softer. Similarly, it was previously observed that the addition of sCT to spherical particles made of polyethylene glycol (PEG) and polyvinylpyrrolidone reduced the degree of crystallinity in the particles and caused particle wrinkling.[33]

The incorporation of sCT and AAT in the formulation favoured the formation of ACC and resulted in the production of completely amorphous particles, which may be important for the stabilization of these molecules and the prevention of any structural damage during processing and storage.[2] The loading efficiency obtained by this process can be compared to other protein encapsulation methods using $CaCO_3$-based particles. Protein can be loaded into $CaCO_3$ particles by physical adsorption onto pre-formed particle,[8, 63] by co-precipitation of the protein during $CaCO_3$ solidification,[54, 64] or by interfacial reaction, where protein is encapsulated *via* a water-in-oil emulsion into $CaCO_3$ microcapsules.[64] For these different processes the loading efficiency varies greatly depending on the type of protein and the process used. One of the highest loading efficiencies of 64.4 ± 4.1% was obtained by the co-precipitation of the protein (lysozyme) with $CaCO_3$ using supercritical CO_2.[54] Comparatively, our process should be classified as a high efficiency process, which is generally the case for spray-dried products.

After landing in the lungs, the microparticles release sCT which is then absorbed or eliminated from the lungs by clearance mechanisms. sCT bioavailability may be improved by either increasing the sCT

absorption rate or reducing the effect of clearance mechanisms. Depending on the region of the lungs that the particle reaches, the lung clearance mechanisms are different. In the deep peripheral lung the main clearance mechanisms for sCT are proteases activity[65] and macrophage phagocytosis. The release of sCT from the particles was fast and complete within 30 min. ACC is the most soluble form of $CaCO_3$ and dissolves quickly, which should be responsible for the fast sCT release. This fast release is beneficial, as it can prevent sCT macrophage degradation after particle phagocytosis and allows for a high sCT concentration gradient across the lung-blood barrier, facilitating sCT absorption.

sCT displayed non-linear pulmonary PK, leading to an increase in sCT bioavailability with an increase in sCT dose. This non-linear PK obtained after pulmonary nebulisation of sCT solution may involve the saturation of sCT clearance mechanisms. In fact, if above a certain sCT concentration, the elimination rate tends to reach a maximal value and there is no further increase in the elimination rate when sCT concentration increases, then an increase in sCT concentration in the lung must increase its bioavailability. However, from a sCT dose of 200 µg kg^{-1} and above, sCT bioavailability plateaued at around 23 % and T_{max} increased with the sCT dose, suggesting a slow-down of sCT absorption and the action of other, slower clearance mechanisms, resulting in a bioavailability of less than 100%. Likewise, the increase in T_{max} and the limitation of sCT bioavailability to 18.5 ± 3.2 % in the presence of AAT, after nebulisation of sCT and AAT solutions, could be explained by the saturation of sCT absorption mechanisms and the action of clearance mechanisms other than proteases.

Thus, AAT nebulised solution in the lung increased sCT bioavailability by reducing sCT enzymatic degradation. However, sCT bioavailability is limited by its absorption rate drop at high concentration. In the same way, PEGylated sCT delivered by the pulmonary route had 4-times increased bioavailability due to higher proteolytic resistance and partly due to reduction of elimination rate from plasma, but achieved a bioavailability of only 50%.[66] This limitation could also be due to a slowing down of the sCT absorption rate with increasing sCT concentration in the lung and the concomitant action of other elimination mechanisms. sCT administered as sCT-AAT particles had higher bioavailability than sCT delivered as solution with or without AAT but had a similar absorption rate. This suggests that the AAT-loaded composite particles were able to further extend the protective action of AAT in the lungs to clearance mechanisms other than protease.

4. Conclusions

We have succeeded in developing a novel formulation approach to prepare shell-like composite microparticles made of selected polymorphs of calcium carbonate (amorphous, calcite and vaterite), calcium formate and hyaluronan. In this new process, different parameters could be controlled and tuned to adapt the microparticle properties. The first parameter was the organic biopolymer/mineral ($CaCO_3$ and $Ca(HCOO)_2$) ratio, while the second parameter was the solid state nature of the mineral component, crystalline/amorphous ratio and polymorphic properties. These inorganic/organic hybrid microparticles were able to preserve peptide and protein activities and deliver them to the lung. The combination of alpha-1-antitrypsin in composite particles with sCT was able to improve sCT bioavailability 4-fold.

5. Experimental Procedures

Spray Drying: a scheme and more details of the spray drying process are presented in the supporting information (Figure S1). Briefly, two solutions were prepared separately and mixed just before entering the spray dryer nozzle. For the production of sCT and sCT-AAT microparticles, one solution was composed of 0.1% v/v of formic acid, 0.4 g L^{-1} of sCT (for the production of sCT microparticles) or 0.2 g L^{-1} of sCT (for the production of sCT-AAT microparticles) (Polypeptide Laboratories, Sweden), 0.8 g L^{-1} of $Ca(OH)_2$ and 0.2 g L^{-1} of HA (Sigma-Aldrich, Dublin, Ireland). The other solution was made of 2.4 g L^{-1} of $(NH_4)_2CO_3$ for the formulation of sCT microparticle and was supplemented with 0.2 g L^{-1} of AAT for the production of sCT-AAT microparticles. Also, the maximal sCT theoretical loading, calculated without taking into account the volatilisation of excess of $(NH_4)_2CO_3$, or the volatilisation of the ammonia and water formed by the reaction of $(NH_4)_2CO_3$ with $Ca(OH)_2$ that happens concomitantly to the spray drying process, is 10.5% (w/w) and 5.3 % (w/w) for the sCT- microparticles and sCT-AAT microparticles, respectively. If we assume the complete elimination of the volatile compounds, the maximal sCT loading would be 23.8 % (w/w) and 11.9 % (w/w) for the sCT- microparticles and sCT-AAT microparticles, respectively.

Scanning Electron Microscopy (SEM) micrographs of samples were taken using a Tescan Mira XMU (Tescan s.r.o., Czech Republic) electron microscope on samples coated with a gold film. Primary electrons were accelerated under a voltage of 5 – 20 kV. Images were formed from the collection of secondary electrons.[33]

Powder X- ray Diffraction (XRD) was carried out on samples placed in a low background silicon holder. Samples were scanned over a range of 15 – 50 º, 2θ at a step size of 0.05 º s^{-1} using a Rigaku Miniflex II desktop X-ray diffractometer (Rigaku, Tokyo, Japan).[32]

The geometric particle size distributions were determined by laser diffraction using a Malvern Mastersizer 2000 (Malvern Instruments Ltd. Worcestershire, UK) with the Scirocco 2000 dry powder feeder to disperse the particles (n = 3).[33]

Dynamic Vapour Sorption (DVS) experiments were performed on a DVS-1 (SMS Ltd., London, UK) at 25.0 ± 0.1 °C as previously described.[33] The samples were exposed to the following % of relative humidity (RH) profile: 0 to 90 % in 10 % steps and the reverse for desorption. At each stage the sample mass was allowed to reach equilibrium. The amount of water uptake for each RH stage was expressed as a % of the dry sample mass (m_0).

Specific surface area of the samples purged under N_2 overnight at 30 °C (n= 3) was determined by the N_2 adsorption B.E.T. multipoint method, with 6 points in the relative pressure range of 0.1 – 0.3, using a Micromeritics Gemini 2835c (SMS Ltd., London, UK).

Material true density was measured by an AccuPyc 1330 Pycnometer (Micromeritics®) using helium (99.995% purity) to determine the volume of samples which had been dried for 24 h at 30°C under nitrogen flow prior to analysis (n = 2) as previously described.[32]

Attenuated total reflectance (ATR)-FTIR measurements were performed on powders placed on a wedged diamond crystal using a spectrum 400FT spectrometer (PerkinElmer, Ireland). For each spectrum, 32-scan interferograms were collected with 4 cm^{-1} resolution.

Analytical assay: The sCT content of the particles was determined by HPLC assay using a LC module I plus (Waters, UK) chromatographic system with a C18, 15-20 µm, 3.9 x 300 mm column (µbondapak™, Waters, Ireland) and previously validated method.[33] The sCT loading, defined as the mass of sCT divided by the total mass of particles, was measured in triplicate. sCT release from 5 – 12 mg of microparticles was performed at 37 °C in 5 mL phosphate buffer saline pH = 7.4 containing 0, 1 or 10 (*N*-α-benzoyl-l-arginine ethyl ester – BAEE) units trypsin per mL. After centrifugation, 100 µL of samples were taken at different time points, diluted in acid solution and assayed for sCT concentration. Fresh buffer was added after each sampling.

The calcium content of the particles was determined based on the interaction of calcium with o-cresolphthalein complexone chromogenic agent. Dry powder samples were dissolved in 1% acetic acid solution, then diluted and mixed with 300 µL of reactive solution (1/1 mix of 2-amino, 2-methyl, 1-propanol solution with a concentration of 40 g L^{-1} and o-cresolphthalein solution with a concentration of 0.1 g L^{-1}). Calibration curves were created with standard solutions having calcium concentrations ranging from 0.15 to 0.01 g L^{-1}. Absorbance at 570 nm was measured on a plate reader (FLUOstar OPTIMA, BMG Labtech, Aylesbury, UK).

Pharmacokinetics: The compliance of this study with EC Directive 86/609 was reviewed and approved by the Trinity College Dublin Ethical Committee. Male Wistar rats (BioResources, TCD, Ireland) weighing 350 ± 50 g were anaesthetised by an intraperitoneal (*i.p.*) injection of a mixture of ketamine (Pfizer, Ireland) and medetomidine (Pfizer, Ireland).[32] Then, heparinized permanent polyurethane intravascular tubings were implanted on the day of the experiment for sCT solution administration or for blood sampling.

sCT *i.v.* bolus administrations were performed by injecting sCT solutions at 70 µg mL^{-1} in 0.9% w/v NaCl. Then, anaesthesia was reversed with atipamezole (5 mg kg^{-1} *i.p.*, Pfizer, Ireland). sCT pulmonary bolus administrations were performed by insufflating about 1 – 2 mg of dry powder using a MicroSprayer™ insufflator (model IA–1B, Penn-Century, Philadelphia, PA, USA) or by nebulising 100 µL of sCT solutions in 0.9% w/v NaCl using an AeroProbe™ intracorporeal nebulising catheter.[17] Anesthetised rats were maintained by the upper incisors on a rodent work stand inclined at 45° then a plastic guide was inserted between the vocal cords. The sprayers were introduced into the plastic tube of the rats in the horizontal position and the formulations were administered when they were breathing in. The anaesthetic reversal agent was injected *i.p.* Blood samples (200 µL) were collected in heparinised tubes at the following times: 0; 3; 10; 20; 30; 60; 90; 120; 180 min after sCT administration. Blood was replaced by an equal volume of isotonic solution. Blood samples were centrifuged and plasma was kept frozen at -20 °C until sCT assay was performed using an ELISA kit (S1155, Bachem, UK). Pharmacokinetic parameters were determined for each individual rat using a two-compartment model as previously described.[32]

Statistical data analysis: Data were statistically evaluated by a Student *t*-test, or a one-way analysis of variance (ANOVA) test with a Tukey's multiple comparison test as post-hoc test. Significance level was $\alpha < 0.05$.

Supporting Information.

Spray drying process scheme, FTIR spectra of Ca/HA composite microparticle formulated at different concentrations of HA and loaded with sCT and AAT, TGA thermograms of Ca/HA composite particles, SEM micrographs of composite particles formulated at different concentrations in $(NH_4)_2CO_3$ and different concentration in HA, sCT-AAT Ca/HA composite particle water sorption versus time profiles, water sorption-desorption isotherm and XRD patterns of sCT-AAT and sCT Ca/HA particles after DVS experiments, the aerodynamic diameter (AD) distribution of sCT-AAT-loaded microparticles.

Acknowledgements

This publication has emanated from research conducted with the financial support of Science Foundation Ireland (SFI) under Grant Numbers 07/SRC/B1158 and SFI/12/RC/2275.

References

(1) Patton, J. S.; Byron, P. R. Inhaling Medicines: Delivering Drugs to the Body Through the Lungs. *Nat. Rev. Drug Discovery* **2007,** *6* (1), 67-74.

(2) Yu, L. Amorphous Pharmaceutical Solids: Preparation, Characterization And Stabilization. *Adv. Drug Delivery Rev.* **2001,** *48* (1), 27-42.

(3) Gordon, M.; Taylor, J. S. Ideal Copolymers and the Second ‐ Order Transitions of Synthetic Rubbers. I. Non ‐ Crystalline Copolymers. *J. Appl. Chem.* **1952,** *2* (9), 493-500.

(4) Arakawa, T.; Prestrelski, S. J.; Kenney, W. C.; Carpenter, J. F. Factors Affecting Short-Term and Long-Term Stabilities of Proteins. *Adv. Drug Delivery Rev.* **2001,** *46* (1), 307-326.

(5) Addadi, L.; Raz, S.; Weiner, S. Taking Advantage of Disorder: Amorphous Calcium Carbonate and its Roles in Biomineralization. *Adv. Mater.* **2003,** *15* (12), 959-970.

(6) Raz, S.; Hamilton, P. C.; Wilt, F. H.; Weiner, S.; Addadi, L. The Transient Phase of Amorphous Calcium Carbonate in Sea Urchin Larval Spicules: The Involvement of Proteins and Magnesium Ions in its Formation and Stabilization. *Adv. Funct. Mater.* **2003,** *13* (6), 480-486.

(7) Wolf, G.; Günther, C. Thermophysical Investigations of the Polymorphous Phases of Calcium Carbonate. *J. Therm. Anal. Calorim.* **2001,** *65* (3), 687-698.

(8) Qi, C.; Zhu, Y.-J.; Chen, F. Microwave Hydrothermal Transformation of Amorphous Calcium Carbonate Nanospheres and Application in Protein Adsorption. *ACS Appl. Mater. Interfaces* **2014,** *6* (6), 4310-4320.

(9) Aizenberg, J.; Lambert, G.; Weiner, S.; Addadi, L. Factors Involved in the Formation of Amorphous and Crystalline Calcium Carbonate: A Study of an Ascidian Skeleton. *J. Am. Chem. Soc.* **2002,** *124* (1), 32-39.

(10) Aizenberg, J.; Weiner, S.; Addadi, L. Coexistence of Amorphous and Crystalline Calcium Carbonate in Skeletal Tissues. *Connect. Tissue Res.* **2003,** *44* (1), 20-25.

(11) Politi, Y.; Arad, T.; Klein, E.; Weiner, S.; Addadi, L. Sea Urchin Spine Calcite Forms Via a Transient Amorphous Calcium Carbonate Phase. *Science* **2004,** *306* (5699), 1161-1164.

(12) Grunenfelder, L. K.; Herrera, S.; Kisailus, D. Crustacean-Derived Biomimetic Components and Nanostructured Composites. *Small* **2014,** *10* (16), 3207-3232.

(13) Lakshminarayanan, R.; Loh, X. J.; Gayathri, S.; Sindhu, S.; Banerjee, Y.; Kini, R. M.; Valiyaveettil, S. Formation of Transient Amorphous Calcium Carbonate Precursor in Quail Eggshell Mineralization: an In Vitro Study. *Biomacromolecules* **2006,** *7* (11), 3202-3209.

(14) Mahamid, J.; Sharir, A.; Addadi, L.; Weiner, S. Amorphous Calcium Phosphate is a Major Component of the Forming Fin Bones of Zebrafish: Indications for an Amorphous Precursor Phase. *Proc. Natl. Acad. Sci. U. S. A.* **2008,** *105* (35), 12748-12753.

(15) Bentov, S.; Weil, S.; Glazer, L.; Sagi, A.; Berman, A. Stabilization of Amorphous Calcium Carbonate by Phosphate Rich Organic Matrix Proteins and by Single Phosphoamino Acids. *J. Struct. Biol.* **2010,** *171* (2), 207-215.

(16) Akiva-Tal, A.; Kababya, S.; Balazs, Y. S.; Glazer, L.; Berman, A.; Sagi, A.; Schmidt, A. In Situ Molecular NMR Picture of Bioavailable Calcium Stabilized as Amorphous CaCO3 Biomineral in Crayfish Gastroliths. *Proc. Natl. Acad. Sci. U. S. A.* **2011,** *108* (36), 14763-14768.

(17) Pouget, E. M.; Bomans, P. H. H.; Goos, J. A. C. M.; Frederik, P. M.; De With, G.; Sommerdijk, N. A. J. M. The Initial Stages of Template-Controlled CaCO3 Formation Revealed by Cryo-TEM. *Science* **2009,** *323* (5920), 1455-1458.

(18) Politi, Y.; Metzler, R. A.; Abrecht, M.; Gilbert, B.; Wilt, F. H.; Sagi, I.; Addadi, L.; Weiner, S.; Gilbert, P. Transformation Mechanism of Amorphous Calcium Carbonate into Calcite in the Sea Urchin Larval Spicule. *Proc. Natl. Acad. Sci. U. S. A.* **2008,** *105* (50), 20045-20045.

(19) Radha, A. V.; Forbes, T. Z.; Killian, C. E.; Gilbert, P. U. P. A.; Navrotsky, A. Transformation and Crystallization Energetics of Synthetic and Biogenic Amorphous Calcium Carbonate. *Proc. Natl. Acad. Sci. U. S. A.* **2010,** *107* (38), 16438-16443.

(20) Bassett, D. C.; Marelli, B.; Nazhat, S. N.; Barralet, J. E. Stabilization of Amorphous Calcium Carbonate with Nanofibrillar Biopolymers. *Adv. Funct. Mater.* **2012,** *22* (16), 3460-3469.

(21) Arias, J. L.; Fernández, M. a. S. Polysaccharides and Proteoglycans in Calcium Carbonate-based Biomineralization. *Chem. Rev.* **2008,** *108* (11), 4475-4482.

(22) Ros, M.; Casciaro, R.; Lucca, F.; Troiani, P.; Salonini, E.; Favilli, F.; Quattrucci, S.; Sher, D.; Assael, B. M. Hyaluronic Acid Improves the Tolerability of Hypertonic Saline in the Chronic Treatment of Cystic Fibrosis Patients: A Multicenter, Randomized, Controlled Clinical Trial. *J. Aerosol Med. Pulm. Drug Delivery* **2014,** *27* (2), 133-137.

(23) Monk, R.; Graves, M.; Williams, P.; Strange, C. Inhaled Alpha 1-Antitrypsin: Gauging Patient Interest in a New Treatment. *COPD* **2013,** *10* (4), 411-415.

(24) Ridha, F. N.; Manovic, V.; Wu, Y.; Macchi, A.; Anthony, E. J. Post-Combustion CO_2 Capture by Formic Acid-Modified CaO-Based Sorbents. *Int. J. Greenhouse Gas Control* **2013,** *16* (0), 21-28.

(25) Al-Hosney, H. A.; Carlos-Cuellar, S.; Baltrusaitis, J.; Grassian, V. H. Heterogeneous Uptake and Reactivity of Formic Acid on Calcium Carbonate Particles: A Knudsen Cell Reactor, FTIR and SEM Study. *Phys. Chem. Chem. Phys.* **2005,** *7* (20), 3587-3595.

(26) Vagenas, N. V.; Gatsouli, A.; Kontoyannis, C. G. Quantitative Analysis of Synthetic Calcium Carbonate Polymorphs using FT-IR Spectroscopy. *Talanta* **2003,** *59* (4), 831-836.

(27) Foran, E.; Weiner, S.; Fine, M. Biogenic Fish-gut Calcium Carbonate is a Stable Amorphous Phase in the Gilt-head Seabream, Sparus aurata. *Sci. Rep.* **2013,** *3*, 1-5.

(28) Ihli, J.; Wong, W. C.; Noel, E. H.; Kim, Y.-Y.; Kulak, A. N.; Christenson, H. K.; Duer, M. J.; Meldrum, F. C. Dehydration and Crystallization of Amorphous Calcium Carbonate in Solution and in Air. *Nat. Commun.* **2014,** *5*, 1-10.

(29) Wilson, R.; Elliott, J.; Dowker, S. Formate Incorporation in the Structure of Ca-Deficient Apatite: Rietveld Structure Refinement. *J. Solid State Chem.* **2003,** *174* (1), 132-140.

(30) Puri, V.; Dantuluri, A. K.; Kumar, M.; Karar, N.; Bansal, A. K. Wettability and Surface Chemistry of Crystalline and Amorphous Forms of a Poorly Water Soluble Drug. *Eur. J. Pharm. Sci.* **2010,** *40* (2), 84-93.

(31) Bianco, S.; Tewes, F.; Tajber, L.; Caron, V.; Corrigan, O. I.; Healy, A. M. Bulk, Surface Properties and Water Uptake Mechanisms of Salt/Acid Amorphous Composite Systems. *Int. J. Pharm.* **2013,** *456* (1), 143-52.

(32) Tewes, F.; Gobbo, O. L.; Amaro, M. I.; Tajber, L.; Corrigan, O. I.; Ehrhardt, C.; Healy, A. M. Evaluation of HPβCD-PEG Microparticles for Salmon Calcitonin Administration via Pulmonary Delivery. *Mol. Pharmaceutics* **2011,** *8* (5), 1887-1898.

(33) Tewes, F.; Tajber, L.; Corrigan, O. I.; Ehrhardt, C.; Healy, A. M. Development and Characterisation of Soluble Polymeric Particles for Pulmonary Peptide Delivery. *Eur. J. Pharm. Sci.* **2010,** *41* (2), 337-352.

(34) Matahwa, H.; Ramiah, V.; Sanderson, R. D. Calcium Carbonate Crystallization in the Presence of Modified Polysaccharides and Linear Polymeric Additives. *J. Cryst. Growth* **2008,** *310* (21), 4561-4569.

(35) Wang, C.; Zhao, X.; Zhao, J.; Liu, Y.; Sheng, Y.; Wang, Z. Biomimetic Nucleation and Growth of Hydrophobic Vaterite Nanoparticles with Oleic Acid in a Methanol Solution. *Appl. Surf. Sci.* **2007,** *253* (10), 4768-4772.

(36) Saharay, M.; Yazaydin, A. O.; Kirkpatrick, R. J. Dehydration-Induced Amorphous Phases of Calcium Carbonate. *J. Phys. Chem. B* **2013,** *117* (12), 3328-36.

(37) Raz, S.; Testeniere, O.; Hecker, A.; Weiner, S.; Luquet, G. Stable Amorphous Calcium Carbonate is the Main Component of the Calcium Storage Structures of the Crustacean Orchestia Cavimana. *Biol. Bull.* **2002,** *203* (3), 269-274.

(38) Pitarresi, G.; Craparo, E. F.; Palumbo, F. S.; Carlisi, B.; Giammona, G. Composite Nanoparticles Based on Hyaluronic Acid Chemically Cross-Linked with α,β-Polyaspartylhydrazide. *Biomacromolecules* **2007,** *8* (6), 1890-1898.

(39) Lee, Y.-H.; Sinko, P. J. Oral Delivery Of Salmon Calcitonin. *Adv. Drug Delivery Rev.* **2000,** *42* (3), 225-238.

(40) Vehring, R.; Foss, W. R.; Lechuga-Ballesteros, D. Particle Formation in Spray Drying. *J. Aerosol Sci.* **2007,** *38* (7), 728-746.

(41) Ihli, J.; Kim, Y.-Y.; Noel, E. H.; Meldrum, F. C. The Effect of Additives on Amorphous Calcium Carbonate (ACC): Janus Behavior in Solution and the Solid State. *Adv. Funct. Mater.* **2013,** *23* (12), 1575-1585.

(42) Aizenberg, J.; Lambert, G.; Addadi, L.; Weiner, S. Stabilization of Amorphous Calcium Carbonate by Specialized Macromolecules in Biological and Synthetic Precipitates. *Adv. Mater.* **1996,** *8* (3), 222-226.

(43) Raiteri, P.; Gale, J. D. Water is the Key to Nonclassical Nucleation of Amorphous Calcium Carbonate. *J. Am. Chem. Soc.* **2010,** *132* (49), 17623-17634.

(44) Saharay, M.; James Kirkpatrick, R. Onset of Orientational Order in Amorphous Calcium Carbonate (ACC) upon Dehydration. *Chem. Phys. Lett.* **2014,** *591* (0), 287-291.

(45) Rodriguez-Blanco, J. D.; Shaw, S.; Benning, L. G. The Kinetics and Mechanisms of Amorphous Calcium Carbonate (ACC) Crystallization to Calcite, via vaterite. *Nanoscale* **2011,** *3* (1), 265-271.

(46) Ogino, T.; Suzuki, T.; Sawada, K. The Rate and Mechanism of Polymorphic Transformation of Calcium Carbonate in Water. *J. Cryst. Growth* **1990,** *100* (1), 159-167.

(47) Sand, K.; Yang, M.; Makovicky, E.; Cooke, D. J.; Hassenkam, T.; Bechgaard, K.; Stipp, S. Binding of Ethanol on Calcite: The Role of the OH Bond and its Relevance to Biomineralization. *Langmuir* **2010,** *26* (19), 15239-15247.

(48) Ihli, J.; Kulak, A. N.; Meldrum, F. C. Freeze-Drying Yields Stable and Pure Amorphous Calcium Carbonate (ACC). *Chem. Commun.* **2013,** *49* (30), 3134-3136.

(49) Gebauer, D.; Gunawidjaja, P. N.; Ko, J.; Bacsik, Z.; Aziz, B.; Liu, L.; Hu, Y.; Bergström, L.; Tai, C. W.; Sham, T. K. Proto ‐ Calcite and Proto ‐ Vaterite in Amorphous Calcium Carbonates. *Angew. Chem.* **2010,** *122* (47), 9073-9075.

(50) Pudipeddi, M.; Serajuddin, A. Trends in Solubility of Polymorphs. *J. Pharm. Sci.* **2005,** *94* (5), 929-939.

(51) Butler, M. F.; Glaser, N.; Weaver, A. C.; Kirkland, M.; Heppenstall-Butler, M. Calcium Carbonate Crystallization in the Presence of Biopolymers. *Cryst. Growth Des.* **2006,** *6* (3), 781-794.

(52) Dickinson, S. R.; McGrath, K. Switching Between Kinetic and Thermodynamic Control: Calcium Carbonate Growth in the Presence of a Simple Alcohol. *J. Mater. Chem.* **2003,** *13* (4), 928-933.

(53) Dickinson, S. R.; Henderson, G. E.; McGrath, K. M. Controlling the Kinetic Versus Thermodynamic Crystallisation of Calcium Carbonate. *J. Cryst. Growth* **2002,** *244* (3–4), 369-378.

(54) M.-K. Tran, L. N. H., B. Calvignac, T. Beuvier, F. Tewes, G.J.-R. Delcroix, F. Hindré, F. Boury Lysozyme Encapsulation Within PLGA and CaCO3 Microparticles Using Supercritical CO2 Medium. *J. Supercrit. Fluids* **2013,** *79*, 159-169.

(55) Carvalho, T. C.; Peters, J. I.; Williams III, R. O. Influence of Particle Size on Regional Lung Deposition – What Evidence is there? *Int. J. Pharm.* **2011,** *406* (1–2), 1-10.

(56) Healy, A. M.; Amaro, M. I.; Paluch, K. J.; Tajber, L. Dry Powders for Oral Inhalation Free of Lactose Carrier Particles. *Adv. Drug Delivery Rev.* **2014,** *75*, 32-52.

(57) Shekunov, B.; Chattopadhyay, P.; Tong, H. Y.; Chow, A. L. Particle Size Analysis in Pharmaceutics: Principles, Methods and Applications. *Pharm. Res.* **2007,** *24* (2), 203-227.

(58) DeCarlo, P. F.; Slowik, J. G.; Worsnop, D. R.; Davidovits, P.; Jimenez, J. L. Particle Morphology and Density Characterization by Combined Mobility and Aerodynamic Diameter Measurements. Part 1: Theory. *Aerosol Sci. Technol.* **2004,** *38* (12), 1185-1205.

(59) Tsapis, N.; Bennett, D.; Jackson, B.; Weitz, D. A.; Edwards, D. A. Trojan Particles: Large Porous Carriers of Nanoparticles for Drug Delivery. *Proc. Natl. Acad. Sci. U. S. A.* **2002,** *99* (19), 12001-12005.

(60) Tewes, F.; Paluch, K. J.; Tajber, L.; Gulati, K.; Kalantri, D.; Ehrhardt, C.; Healy, A. M. Steroid/Mucokinetic Hybrid Nanoporous Microparticles for Pulmonary Drug Delivery. *Eur. J. Pharm. Biopharm.* **2013,** *85* (3), 604-613.

(61) Amaro, M. I.; Tajber, L.; Corrigan, O. I.; Healy, A. M. Optimisation of Spray Drying Process Conditions for Sugar Nanoporous Microparticles (NPMPs) Intended for Inhalation. *Int. J. Pharm.* **2011,** *421* (1), 99-109.

(62) Chan, H. K.; Clark, A. R.; Feeley, J. C.; Kuo, M. C.; Lehrman, S. R.; Pikal‐Cleland, K.; Miller, D. P.; Vehring, R.; Lechuga‐Ballesteros, D. Physical Stability of Salmon Calcitonin Spray‐Dried Powders for Inhalation. *J. Pharm. Sci.* **2004,** *93* (3), 792-804.

(63) Petrov, A. I.; Volodkin, D. V.; Sukhorukov, G. B. Protein-Calcium Carbonate Coprecipitation: a Tool for Protein Encapsulation. *Biotechnol. Prog.* **2005,** *21* (3), 918-25.

(64) Hassani, L. N.; Hindré, F.; Beuvier, T.; Calvignac, B.; Lautram, N.; Gibaud, A.; Boury, F. Lysozyme Encapsulation into Nanostructured $CaCO_3$ Microparticles Using a Supercritical CO_2 Process and Comparison with the Normal Route. *J. Mater. Chem. B* **2013,** *1* (32), 4011-4019.

(65) Garcia-Verdugo, I.; Descamps, D.; Chignard, M.; Touqui, L.; Sallenave, J.-M. Lung Protease/Anti-Protease Network and Modulation of Mucus Production and Surfactant Activity. *Biochimie* **2010,** *92* (11), 1608-1617.

(66) Youn, Y. S.; Kwon, M. J.; Na, D. H.; Chae, S. Y.; Lee, S.; Lee, K. C. Improved Intrapulmonary Delivery of Site-Specific Pegylated Salmon Calcitonin: Optimization by PEG Size Selection. *J. Controlled Release* **2008,** *125* (1), 68-75.